applied optics

Method for measurement of eccentricity and tilt of lenslet array integral field spectrometer

Jianan Liu,[1,2] Jianjun Chen,[1,2] Jianli Liu,[1,2] Shulong Feng,[1] Jin Yang,[1] Nan Song,[1] Ci Sun,[1] Jicheng Cui,[1,*] and Bayanheshig[1,3]

[1]National Engineering Research Centre for Diffraction Gratings Manufacturing and Application, Changchun Institute of Optics, Fine Mechanics and Physics, Chinese Academy of Sciences, Changchun, Jilin 130033, China
[2]Daheng College, University of Chinese Academy of Sciences, Beijing 100049, China
[3]e-mail: bayin888@sina.com
*Corresponding author: jicheng_cui@163.com

Received 5 June 2018; revised 30 September 2018; accepted 30 September 2018; posted 4 October 2018 (Doc. ID 334429); published 26 October 2018

This paper proposes a more accurate eccentricity and tilt measurement method based on Young's interference experiment. The basic principle of the method is introduced first before the method is simulated. Then the results are obtained when a to-be-adjusted focusing lens with eccentricity and tilt is simulated. The optical sensitivity also is obtained from these simulation results, and the expression for the change in optical path length caused by eccentricity and tilt is analyzed. Use of this method to detect eccentricity and tilt and assist in adjustment of the system allows the instrument to achieve higher accuracy and thus obtain improved imaging quality and spectral resolution.

https://doi.org/10.1364/AO.57.000F50

1. INTRODUCTION

The imaging spectrometer is the result of a combination of imaging technology with spectroscopy [1–3]. This instrument can not only obtain target image information but can also obtain the spectral characteristics of the target material from the acquired spectral image data; it can thus obtain a target's spectral characteristics and confirm its existence and its material composition. This spectrometer has a wide range of applications in meteorology, resource management, and environmental, ecological, and other fields [4,5]. The imaging spectrometers use a slit that constrains the spatial resolution of the target, thus limiting the system's luminous flux and reducing its signal-to-noise ratio [6]. At the same time, the slit imaging spectrometer requires a push sweep or a sweep to obtain all required information, which not only wastes large amounts of observation time but also reduces the system's stability. Lenslet array integral field spectrometry (IFS) is a fast and efficient type of three-dimensional (3D) imaging spectrometer, initially used in astronomy [7]. The lenslet array IFS has no moving parts or slits, so it offers higher stability and can acquire the target 3D data cube more rapidly [8,9]. The spectrometer obtains a spectrum of each spatial element in its fields of view, producing a cube of data corresponding to two spatial (x, y) and one spectral (λ) dimension. It gathers complete information of the celestial body, greatly saving valuable observation time on the telescope, and improves the stability and consistency of the observed data. It has proved to become one of the most effective means for performing 3D imaging spectroscopy and a central focus in present-day technological advances in astronomical instrumentation.

For measurement of the center deviation, there are two main classification methods. The first method is divided into collimated imaging and interferometry and is based on the coherence of the light source used; the other is based on the light propagation method used to separate it into reflective and transmissive measurements. These two methods are crossed with each other to form the four main types of center deviation measurement method [10–15]. The basic principle of reflective collimation imaging measurement is that a self-collimating optical path is used to reflect the center deviation of a measured spherical surface onto the deviation of the target object's quasi image. This method measures the position of the sphere center on the measured surface of the measured lens. Therefore, to determine the deviation of the optical axis of the measured lens from the reference axis, the position of the sphere center on the other surface of the lens must also be obtained. In general, recursive measurement methods are used to obtain the center position of the second face and thus determine the optical axis of the lens and measure the center deviation of the lens. In the transmissive imaging measurement method, the light that is emitted from the index object passes through the optical system into parallel light and is then refracted and imaged using the test lens. If a center deviation is present in the lens under test,

the index image that it produces will deviate from the optical axis. In reflective center interferometry, the reflected light from the surface of the measured lens interferes with the reference light. The center deviation information can then be obtained from the interference pattern. Depending on the difference in position of the reflected light from the lens, the method can be divided into two types: center interferometry–based and edge interferometry–based methods. Transmissive interferometry determines the optical axis of a lens by measuring the two focus lines (measured line) of the lens and then comparing the deviation between the reference axis and the measured line to determine the center deviation of the lens. When the two basic methods of imaging and interferometry are compared, the measurement range for imaging is large, the results are intuitive, fewer components are required to perform the measurements, and the structure is simple, which is conducive to system integration. In contrast, the interferometric range is relatively small, the required structure is more complex, and the processing of the results is more difficult, but the measurement accuracy of interferometry is generally higher than that of the imaging-type measurement method [16–19].

The lenslet array in lenslet array IFS is a binary optical element. Therefore, when compared with traditional imaging spectrometers, the lenslet array IFS is more sensitive to errors such as eccentricity and tilt, and optical adjustment is thus more critical. Use of the method for detection of eccentricity in traditional imaging spectrometers cannot meet the integration requirements of a field-of-view imaging spectrometer. This paper presents a more accurate method for detection of eccentricity and tilt. The proposed method is based on Young's double-slit interference experiment [20]. The eccentricity and tilt of the lens will cause the optical paths of the two interfering light beams to differ, which results in offset of the interference fringes. This method converts the eccentricity and tilt distance errors into interference fringe offsets, thus allowing the accuracy to reach wavelength order.

2. PRINCIPLE OF THE SYSTEM

A schematic diagram of the optical system of the lenslet array IFS is shown in Fig. 1. The light is converged using the preimaging system and is then incident on the lenslet array. After it passes through the lenslet array, the beam forms a microaperture array at the focal plane of the lenslet array. This microaperture array serves as an entrance aperture to the subsequent spectrometer system and replaces the slit that is used in a conventional imaging spectrometer. The image of the microaperture is collimated, is split using the spectrometer system, and is finally converged onto the detector to form an image of the microaperture array. Because of the dispersion effect of the spectrometer system, the microaperture array is thus actually a 2D array of spectral bands, as shown in Fig. 1. To prevent crosstalk in the optical information that is obtained using the microaperture array, the preimaging system that is placed in front of the microlens array requires an image-side telecentric structure and high telecentricity. In addition, the lenslet array belongs to the group of binary optical elements. During the adjustment process, the lenslet array and the other mirrors require higher eccentricity and higher tilt errors. Therefore,

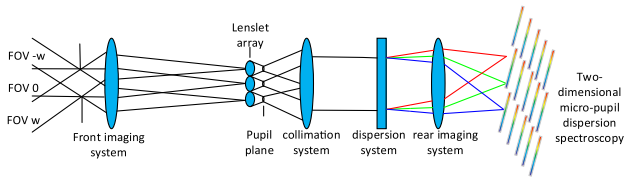

Fig. 1. Schematic diagram of lenslet array IFS.

a measurement method that is more sensitive to eccentricity that is based on Young's interference test method was chosen for this work.

The device used to detect eccentricity and tilt based on Young's interference experiment is shown in Fig. 2. This device is composed of a polychromatic light source, Young's double slit, a high-precision adjustable frame with multiple degrees of freedom, a lens for mounting, an imaging lens, a shock-proof ground structure, and a charge-coupled device (CCD) detector. The light that is emitted by the light source is incident on the double slits of the screen, where the two slits are in close proximity and are equidistant from the light source. The light waves that are emitted from S_1 and S_2 are separated from the same light wave and are both coherent light waves. The two beams are imaged using the imaging lens on the CCD detector behind the lens to be mounted and are superimposed on the CCD detector to form an interference pattern. The changes in the interference fringes are strongly affected by the surrounding environment. Therefore, the entire device setup is mounted on the same antivibration ground structure as the precision turntable to ensure that the device maintains the same amplitude as the examined mirror, which thus greatly reduces the errors that are caused by vibration.

S_1 and S_2 represent the intersections of the slits and the meridian plane. Assume here that point P is an arbitrary point located on the CCD. For convenience in the calculations, illumination by a monochromatic light source is initially considered. When the two interference light beams pass through the lens under test, the intensity of the light that is produced by their superposition at point P is

$$I = I_1 + I_2 + 2\sqrt{I_1 I_2}\cos\delta. \tag{1}$$

Here, I_1 and I_2 are the light intensities of the two light waves incident on the screen, and δ is the optical path difference. If the widths of the two slits in the experimental device are equal, then $I_1 = I_2 = I_0$. At the same time, the distances from the

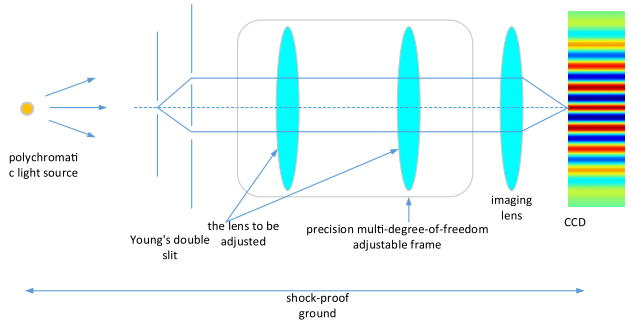

Fig. 2. Structural diagram of the device setup.

two slits to the light source are also equal, which means that the vibrations at the two slits are in the same phase. The phase difference between the light waves at point P is dependent on the difference in the optical paths from points S_1 and S_2 to point P. Let the distances from S_1 and S_2 to point P be r_1 and r_2, respectively; then, the optical path difference at point P is $D = n(r_2 - r_1)$, so the phase difference is

$$\delta = 2\pi \frac{n(r_2 - r_1)}{\lambda}. \tag{2}$$

n is the refractive index of the medium, and λ is the wavelength in a vacuum. Bringing Eq. (2) into Eq. (1) allows the light intensity expression to be written as

$$I = 2I_0 + 2I_0 \cos\left[2\pi n \frac{r_2 - r_1}{\lambda}\right] = 4I_0 \cos^2\left[\frac{\pi n(r_2 - r_1)}{\lambda}\right]. \tag{3}$$

The light intensity at point P is determined by difference in the optical paths from points S_1 and S_2 to point P. Over the entire diffraction screen, when some points meet the following conditions,

$$D = r_2 - r_1 = m\lambda \qquad m = 0, \pm 1, \pm 2, \ldots, \tag{4}$$

then the light intensity at these points has a maximum value of $I = 4I_0$; when other points meet the following conditions,

$$D = r_2 - r_1 = \left(m + \frac{1}{2}\right)\lambda \qquad m = 0, \pm 1, \pm 2, \ldots, \tag{5}$$

then the light intensity at these points has a minimum value of $I = 0$. At the remaining points, the light intensity has a value between 0 and $4I_0$ [21].

The simulation of Young's double-slit interference under illumination by monochromatic light is shown in Fig. 3(a). When there is no lens eccentricity to be detected in the optical path that detects decentering of the lens, the position of the zero-order major maximum is the center of the lens. However, because it is difficult to distinguish the dominant position in the interferogram of Young's double-slit interference experiment when simulated using monochromatic light, polychromatic light is selected for the simulation. Young's double-slit interferogram of complex-colored light is shown in Fig. 3(b). It is easy to see that, when compared with Young's interference fringes from monochromatic light, the center position of the lens can be found more easily in the simulation using multicolored light, thereby enabling more accurate determination of the amount of variation in the interference fringes caused by eccentricity and tilt. Therefore, we use Young's interference method based on polychromatic light to measure the eccentricity during adjustment of the optical system.

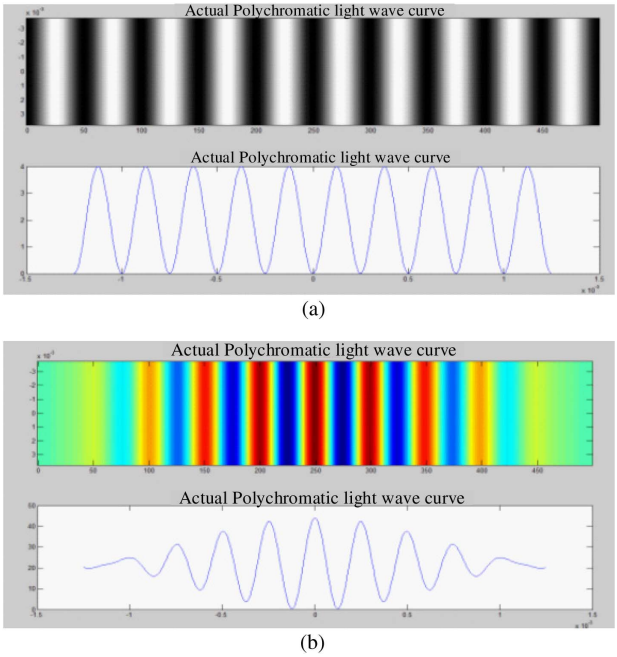

Fig. 3. (a) Simulation results obtained using monochromatic light; (b) simulation results obtained using polychromatic light.

3. SIMULATION OF ECCENTRICITY AND TILT

In accordance with the model established above, the variation produced by the interference fringes is simulated under conditions of eccentricity or tilt of the lens. First, to maintain the above optical path difference of zero, an eccentricity of only 1 μm is applied to the lens to be mounted, and the variation of the interference fringes is shown in Fig. 4. From Fig. 4(a), we see that there is a movement of approximately 0.25 stripe widths in the zero-order dominant position of the interference fringe. When the lens is given a tilt of 2.5e – 8°, a translation of 0.2 fringe-widths occurs at the zero-order dominant position of the interference fringe, as shown in Fig. 4(b). The main cause of the variation in the interference fringes is that the optical path difference between the two interference light beams changes. The eccentricity or tilt of the lens to be adjusted causes the lens position to change. After the light that is emitted from the Young's double slits passes through the lens to be mounted, the optical path difference between the two light beams when convergent on the CCD is no longer zero.

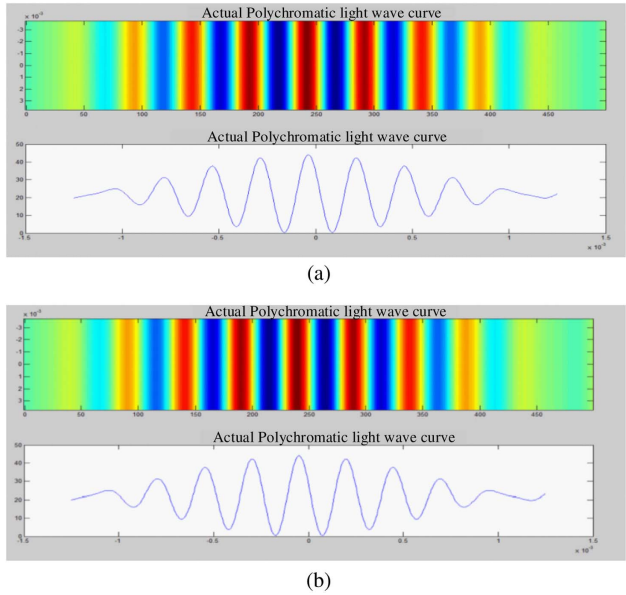

Fig. 4. (a) Simulation of the eccentricity. (b) Simulation of the tilt.

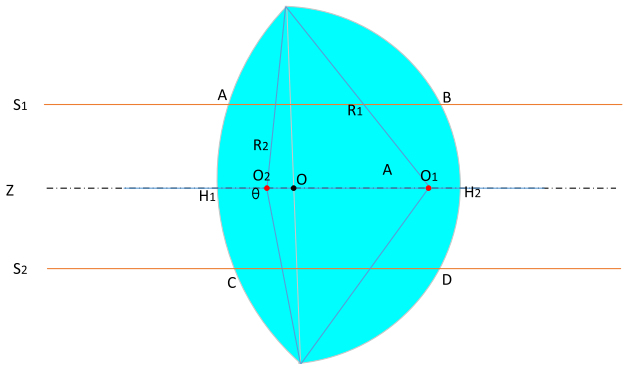

Fig. 5. Optical schematic view of lens without eccentricity or tilt.

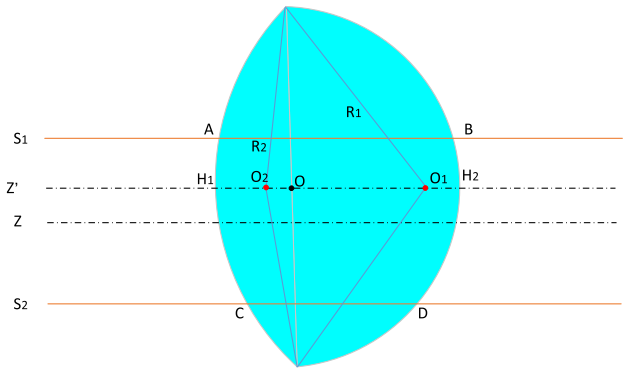

Fig. 6. Optical schematic view of the lens with eccentricity.

The changes on the optical path difference caused by the eccentricity and the tilt of the lens will be analyzed separately. Figure 5 shows an optical schematic view of the lens when there is no eccentricity or tilt present. Z is the optical axis, s_1 and s_2 are the intersections of the plane where the slit is located with the meridian plane, and the Young's double-slit distance is $2d$. A and B are the intersection coordinates of s_1 and the lens to be mounted, where these coordinates are $A(x_a, y_a)$ and $B(x_b, y_b)$, respectively, and C and D are the intersection coordinates of s_2 and the lens to be mounted, where the coordinates are $C(x_c, y_c)$ and $D(x_d, y_d)$, respectively. O_1 is the center of the circle in which the front surface of the lens to be mounted is located, and R_1 is its radius of curvature, while O_2 is the center of the circle in which the rear surface of the lens to be mounted is located and R_2 is its radius of curvature. H_1 and H_2 represent the intersections of the optical axis Z and the front and rear surfaces of the lens to be mounted, respectively, and the point O is the point of intersection of the optical axis and the front and rear surfaces of the lens. The coordinate system is established using the H_1 point as the origin. The O_1 point coordinate is $O_1(L_{H_1O_1}, 0)$, and the O_2 point coordinate is $O_2(L_{H_1O_2}, 0)$. The equation for circle O_1 is then,

$$(x - L_{H_1O_1})^2 + y^2 = R_1^2. \tag{6}$$

The equation for circle O_2 is

$$(x - L_{H_1O_2})^2 + y^2 = R_2^2. \tag{7}$$

The equations for s_1 and s_2 are

$$y = d, \tag{8}$$

$$y = -d. \tag{9}$$

$L_{H_1O_1}$ and $L_{H_1O_2}$ are known quantities. Equations (6) and (8) can be used to obtain the abscissa of point A, x_a, as

$$x_a = L_{H_1O_1} + \sqrt{R_1^2 - d^2}. \tag{10}$$

Similarly, the abscissa of point B, x_b, is

$$x_b = L_{H_1O_2} + \sqrt{R_2^2 - d^2}. \tag{11}$$

When there is eccentricity in the lens to be adjusted, as shown in Fig. 6, the eccentric displacement is denoted by m. In this case, the coordinates of point O_1 are $O_1(L_{H_1O_1}, m)$, the coordinates of point O_2 are $O_2(L_{H_1O_1}, m)$, and the equations for circle O_1 and circle O_2 after the eccentricity are

$$(x - L_{H_1O_1})^2 + (y - m)^2 = R_1^2, \tag{12}$$

$$(x - L_{H_1O_2})^2 + (y - m)^2 = R_2^2. \tag{13}$$

Using the equations for circle O_1, circle O_2, s_1, and s_2, the abscissas of points A, B, C, and D can then be obtained. The corresponding. x_a, x_b, x_c, and x_d values are

$$x_a = L_{H_1O_1} + \sqrt{R_1^2 - (d - m)^2}, \tag{14}$$

$$x_b = L_{H_1O_2} + \sqrt{R_2^2 - (d - m)^2}, \tag{15}$$

$$x_c = L_{H_1O_1} + \sqrt{R_1^2 - (d + m)^2}, \tag{16}$$

$$x_d = L_{H_1O_2} + \sqrt{R_2^2 - (d + m)^2}. \tag{17}$$

Here, L_{AB} and L_{CD} are

$$L_{AB} = (L_{H_1O_2} - L_{H_1O_1}) + \left[\sqrt{R_2^2 - (d - m)^2} - \sqrt{R_1^2 - (d - m)^2}\right], \tag{18}$$

$$L_{CD} = (L_{H_1O_2} - L_{H_1O_1}) + \left[\sqrt{R_2^2 - (d + m)^2} - \sqrt{R_1^2 - (d + m)^2}\right]. \tag{19}$$

The expression for the optical path difference Δ_t caused by the eccentricity is

$$\begin{aligned}\Delta_d &= (L_{CD} - L_{AB}) + n(L_{AB} - L_{CD}) \\ &= (n - 1)(L_{AB} - L_{CD}) \\ &= (n - 1)\left(\sqrt{R_2^2 - (d - m)^2} - \sqrt{R_1^2 - (d - m)^2}\right. \\ &\quad \left. - \sqrt{R_2^2 - (d + m)^2} + \sqrt{R_1^2 - (d + m)^2}\right).\end{aligned} \tag{20}$$

When there is a tilt of the lens, as shown in Fig. 7, the tilt angle is θ, and the center coordinates of both circle O_1 and circle O_2 change. Their tilted center coordinates are $O_1(L_{H_1O_1}\cos\theta,$

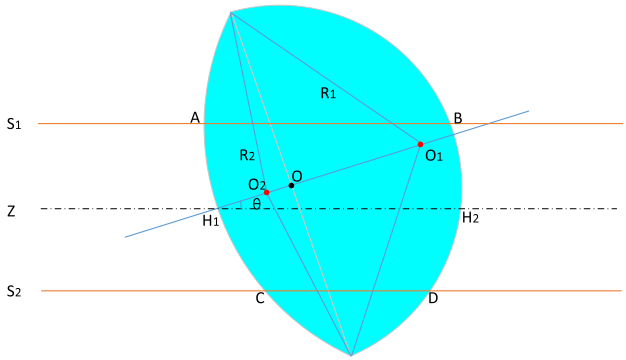

Fig. 7. Optical schematic view of the lens with tilt.

$L_{H_1O_1}\sin\theta)$ and $O_2(L_{H_1O_2}\cos\theta, L_{H_1O_2}\sin\theta)$, respectively. The equations of these sloping circles, O_1 and O_2, are

$$(x - L_{H_1O_1}\cos\theta)^2 + (y - L_{H_1O_1}\sin\theta)^2 = R_1^2, \tag{21}$$

$$(x - L_{H_1O_2}\cos\theta)^2 + (y - L_{H_1O_2}\sin\theta)^2 = R_2^2. \tag{22}$$

Using the equations for circle O_1, circle O_2, s_1, and s_2, the abscissas of points A, B, C, and D can then be obtained.

The corresponding values of x_a, x_b, x_c, and x_d are

$$x_a = L_{H_1O_1}\cos\theta + \sqrt{R_1^2 - (d - L_{H_1O_1}\sin\theta)^2}, \tag{23}$$

$$x_b = L_{H_1O_2}\cos\theta + \sqrt{R_2^2 - (d - L_{H_1O_2}\sin\theta)^2}, \tag{24}$$

$$x_c = L_{H_1O_1}\cos\theta + \sqrt{R_1^2 - (d + L_{H_1O_1}\sin\theta)^2}, \tag{25}$$

$$x_d = L_{H_1O_2}\cos\theta + \sqrt{R_2^2 - (d + L_{H_1O_2}\sin\theta)^2}. \tag{26}$$

Here, L_{AB} and L_{CD} are

$$\begin{aligned} L_{AB} = {} & (L_{H_1O_2} - L_{H_1O_1})\cos\theta \\ & + \sqrt{R_2^2 - (d - L_{H_1O_2}\sin\theta)^2} \\ & - \sqrt{R_1^2 - (d - L_{H_1O_1}\sin\theta)^2}, \end{aligned} \tag{27}$$

$$\begin{aligned} L_{CD} = {} & (L_{H_1O_2} - L_{H_1O_1})\cos\theta \\ & + \sqrt{R_2^2 - (d + L_{H_1O_2}\sin\theta)^2} \\ & - \sqrt{R_1^2 - (d + L_{H_1O_1}\sin\theta)^2}. \end{aligned} \tag{28}$$

The expression for the optical path difference Δ_t that is caused by the tilt is

$$\begin{aligned} \Delta_t = {} & (n-1) \\ & \times \left(\sqrt{R_2^2 - (d - L_{H_1O_2}\sin\theta)^2} \right. \\ & - \sqrt{R_1^2 - (d - L_{H_1O_1}\sin\theta)^2} \\ & - \sqrt{R_2^2 - (d + L_{H_1O_2}\sin\theta)^2} \\ & \left. + \sqrt{R_1^2 - (d + L_{H_1O_1}\sin\theta)^2} \right). \end{aligned} \tag{29}$$

MATLAB software was used to simulate the influence of the eccentricity and the tilt on the interference fringes, and the weights, a and b, of the influence of the eccentricity and the tilt, respectively, on the interference fringe variations were obtained. Finally, we obtain the following optical path difference Δ when the lens to be installed has both eccentricity and tilt:

$$\Delta = a\Delta_d + b\Delta_t. \tag{30}$$

4. OPTICAL ACCURACY

The distance between two adjacent bright stripes or between two dark stripes is called the fringe spacing and is denoted by e. The expression for the spacing e of the interference fringes in Young's double-slit interference experiment is

$$e = \frac{D}{d}\lambda, \tag{31}$$

where D is the distance from the observation point to the double seam and d is the distance between Young's double seams. λ is the center wavelength of the observation band, and when $D = 1m$, $d = 0.5$ mm, and $\lambda = 0.587$ μm, then the stripe width e is 1.174 mm. The results of the above simulations show that the lens is translated by 1 μm, the zero-order major translation is approximately 293.5 μm, the lens tilt is 2.5e − 8°, and the zero-order major translation is approximately 234.8 μm. Because the electronics subdivision technology can reach 50 nm, the optical precision can be converted to 0.0002 μm. The actual polychromatic light wave curve is shown in Fig. 8.

To determine whether or not the eccentricity and tilt of the to-be-adjusted lens satisfies the system requirements, an evaluation function must be defined to evaluate the adjustment error. σ^2 is defined as the evaluation function for the system and is expressed as

$$\sigma^2 = \sum_{i=-N}^{+N} (y_{x_{0-i}} - y_{x_{0+i}})^2. \tag{32}$$

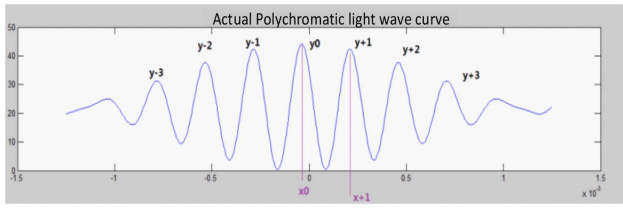

Fig. 8. Actual polychromatic light wave curve.

When x_0 is the maximum coordinate, x_{0-i} is the interference fringe of $-i$, which is reflected on the CCD detector as the pixel coordinate, and y is the gray value of the stripe. For different installation accuracy requirements, different values can be set for σ^2. If the σ^2 value in the adjustment process is within the set range, the adjustment can be considered to meet the accuracy requirements. If the value of σ^2 exceeds the preset precision value, this means that the eccentricity does not reach the expected requirement, and it is thus necessary to continue to adjust the attitude of the lens until the preset precision value is satisfied.

5. CONCLUSIONS

The traditional method for measurement of the eccentricity of a lens to be installed cannot meet the lenslet array IFS mounting accuracy requirements, so this paper proposes a method with higher optical precision based on Young's double-slit interference experiment to measure lens eccentricity. First, the basic principles of the method were introduced, and then a theoretical model for simulation was established. The monochromatic light model and the polychromatic light model were compared. Then, polychromatic light was selected to simulate the eccentricity and the tilt of the lens. From the results of the simulation analysis, the optical sensitivity was then obtained. The optical path difference that was generated by the eccentricity was analyzed, and finally the error evaluation function was given. When different systems are to be installed, there will also be different eccentricity requirements, so different error accuracy values can be preset. When the adjustment function exceeds the relevant preset precision value during the adjustment process, this indicates that the eccentricity does not meet the system's requirements, and it is then necessary to continue to adjust the attitude of the lens to be mounted until the accuracy requirement is satisfied. The method based on the eccentricity of Young's double-slit interferometric system is not only suitable for adjustment of the microlens array integral to the field-of-view imaging spectrometer but is also applicable to other transmissive systems that require high eccentricity accuracy.

Funding. National Major Scientific Instrument and Equipment Development Projects (2014YQ120351); Chinese Finance Ministry for the National R&D Projects for the National Natural Science Foundation of China (NSFC) (61505204); Ministry of National Science and Technology for National Key Basic Research Program of China (2014CB049500); Changchun Science and Technology Project (12ZX23); Jilin Major Province Science & Technology Development Program Project (20140203011GX); Chinese Finance Ministry for the National R&D Projects for Key Scientific Instruments (ZDYZ2008-1); Jilin Outstanding Youth Project in China (20170520167JH).

REFERENCES

1. A. Eberhagen, "A very rapidly scanning monochromator with low internal losses but high spectral resolution and repetition rate for millimetre and submillimetre wavelengths and below," Infrared. Phys. **19**, 389–394 (1979).
2. S. H. Deng, "Development of intelligentized multi-grating monochromator," J. Infrared Millimeter Waves **21**, 133–137 (2002).
3. B. H. Hamadani, J. Roller, and B. Dougherty, "Absolute spectral responsivity measurements of solar cells by a hybrid optical technique," Appl. Opt. **52**, 5184–5193 (2013).
4. Z. X. Wang, "Principle and application of the measurement of the centering errors in optical system," Opt. Technol. **3**, 67–77 (1998).
5. Y. Tang, C. Zhang, H. Jia, Y. Nan, F. Li, and J. Stenberg, "Theoretical and experimental study on anamorphosis correction of Czerny–Turner imaging spectrometers," Appl. Opt. **54**, 2507–2513 (2015).
6. J. E. Larkin, A. Quirrenbach, A. Krabbe, T. Aliado, M. Barczys, G. Brims, J. Canfield, T. Gasaway, D. LaFreniere, N. Magnone, G. Skulason, M. Spencer, D. Sprayberry, and J. Weiss, "OSIRIS, an infrared integral field spectrograph for the Keck adaptive optics system," Proc. SPIE **4841**, 1600–1610 (2003).
7. J. Larkin, M. Barczys, A. Krabbe, S. Adkins, T. Aliado, and P. Amico, "OSIRIS: a diffraction limited integral field spectrograph for Keck," Proc. SPIE **6269**, 62691A (2006).
8. J. E. Larkin, "Diffraction limited integral field spectrographs for large telescopes," Proc. SPIE **9192**, 91920C (2014).
9. S. Thibault, "Cryogenic lens design case study: Gemini planet imager spectrograph," Proc. SPIE **8128**, 812802 (2011).
10. Y. Kim, O. Kwon, S. M. Lee, J. Lee, H. Kim, S. Choi, H. S. Park, and Y. Kim, "Set of secondary emission standards for calibration of the spectral responsivity in emission spectroscopy," Appl. Spectrosc. **52**, 1179–1189 (1998).
11. N. Sigrist, D. C. Redding, J. Z. Lou, Y. Zhang, and S. Basinger, "Optical system alignment via optical state estimation using wavefront measurements," Proc. SPIE **5965**, 596524 (2005).
12. H. X. Cao, N. Wu, S. L. Feng, M. Z. Pan, Y. C. Zhang, and J. C. Cui, "Cross-spectral calibration for monochromator and imaging spectrometer," Opt. Precis. Eng. **22**, 2585–2591 (2014).
13. P. Mouroulis, R. O. Green, and D. W. Wilson, "Optical design of a coastal ocean imaging spectrometer," Opt. Express **16**, 9087–9096 (2008).
14. J. Reimers, A. Bauer, K. P. Thompson, and J. P. Rolland, "Freeform spectrometer enabling increased compactness," Light Sci. Appl. **6**, e17036 (2017).
15. M. Kosec, M. Bürmen, D. T. F. Pernuš, and B. Likar, "Characterization of a spectrograph based hyperspectral imaging system," Opt. Express **21**, 12085–12099 (2013).
16. Y. Kim, H. Yang, J. Song, S. Kim, and Y. Lee, "Modeling alignment experiment errors for improved computer-aided alignment," J. Opt. Soc. Korea **17**, 525–532 (2013).
17. J. W. Figoski, T. E. Shrode, and G. F. Moore, "Computer-aided alignment of a wide field, three-mirror, unobscured, high-resolution sensor," Proc. SPIE **1049**, 166–177 (1989).
18. H. Lee, G. B. Dalton, I. A. J. Tosh, and S.-W. Kim, "Computer-guided alignment II: optical system alignment using differential wavefront sampling," Opt. Express **15**, 15424–15437 (2007).
19. J. Pu and C. Cai, "Spectral anomalies in Young's double-slit interference experiment," Opt. Express **12**, 5131–5139 (2004).
20. H. Shi, X. Luo, and C. Du, "Observation of Young's double-slit interference with the three-photon N00N," Opt. Express **19**, 24957–24966 (2011).
21. Q. T. Liang, *Physical Optics* (2008), pp. 78–80.